JOURNAL OF AIRCRAFT
Vol. 47, No. 2, March–April 2010

Controllable Drogue for Automated Aerial Refueling

Walton R. Williamson*
SySense Inc., Burbank, California 91502
Eric Reed†
Arizona Paradrogue Systems, Kingman, Arizona 86401
Gregory J. Glenn‡
SySense Inc., Burbank, California 91502
and
Stephen M. Stecko,§ Jeffrey Musgrave,¶ and John M. Takacs**
The Boeing Company, Long Beach, California 90807

DOI: 10.2514/1.44758

This paper presents a new method for controlling and stabilizing an automated refueling drogue. The drogue automatically stabilizes in the presence of winds or receiver forebody effects using drogue canopy manipulation. This paper reports on a characterization and simulation study in which the stability derivatives of a low-speed drogue were calculated based on wind-tunnel data. A simulation was developed using a pendulum-based hose model combined with the aerodynamic drogue model. An active feedback control system is shown to stabilize and control the drogue to hold a commanded steady-state offset.

Nomenclature

C_A^B	=	cosine rotation matrix to rotate a vector in the A reference frame into the B frame
F^A	=	force acting on a body in the A reference frame
g^T	=	gravity vector in the north–east–down reference frame
I^{BB}	=	rotational moment of inertia of the body
M^A	=	moment acting on a body in the A reference frame
m	=	mass of the body
$Q_B^A \otimes Q_C^B$	=	quaternion rotation from the C frame to the A frame
Q_A^B	=	quaternion representation of a rotation from the A reference frame to the B frame
$\dot{x}$	=	time derivative of the vector x
$\bar{x}$	=	a priori estimate of the parameter
$\hat{x}$	=	a posteriori estimate of the parameter
$\tilde{x}$	=	measurement of the parameter
α	=	angle of attack
β	=	angle of sideslip
δx	=	perturbation about the parameter x (truth minus a priori estimate)
$[\omega\times]$	=	cross-product matrix representation of the vector
ω_{AB}^C	=	angular velocity of the B frame relative to the A frame represented in the C frame

Received 5 April 2009; revision received 19 December 2009; accepted for publication 26 December 2009.

*Principal Investigator, 300 East Magnolia Boulevard, Suite 300. Member AIAA.
†Project Engineer, 5075A Flightline Drive.
‡Research Engineer, 300 East Magnolia Boulevard, Suite 300. Senior Member AIAA.
§Manager, Advanced Aerial Refueling Systems, Boeing Integrated Defensive Systems, 2401 East Wardlow Road, Long Beach, CA 90807.
¶Senior Research Engineer, Boeing Phantom Works, Seattle, WA.
**Senior Principal Engineer, Electro-Optics, Boeing Integrated Defense Systems, 2600 Westminster Boulevard, SL-13, Seal Beach, CA 90740.

I. Introduction

AUTOMATED aerial refueling typically refers to a process in which a receiver aircraft automatically tracks the tanker or drogue systems. For drogue systems, the receiver must perform a rendezvous maneuver to link with the drogue. This paper presents an alternative method in which control effectors in the form of canopy manipulation are added to the refueling drogue. The automatic control system on the drogue commands these actuators to hold a position relative to the tanker and attenuate the influence of wind gusts and disturbances due to receiver impact, as well as to compensate receiver aerodynamic forebody effects that tend to push the drogue away from the receiver. When implemented, the controllable and stabilized drogue could reduce the requirements for navigation and control on the receiver aircraft, enabling rendezvous function at a lower overall system cost.

The control approach taken in this paper is to use drogue canopy manipulation. Drogues are equipped with canopy material attached to the end of the strut-arm basket. This canopy generates drag during flight in the direction of airflow, which acts to lift the drogue coupling into a nearly horizontal position. For the purposes of this paper, canopy manipulation consists of adjusting the local angle of attack of the leading edge of a portion of the drogue canopy to change the location or direction of the localized center of pressure on the canopy, which results in side forces that may be exploited for control. The means of mechanizing this process consists of enabling strut arms attached to the leading edge (foremost) of the canopy and a second set attached to the trailing-edge (aftmost) ring of the canopy and adjusting the angle between these two arms at different locations around the circumference of the drogue. A simple cruciform configuration is examined in this paper to minimize the number of actuators required to four. Note that for low-speed drogues, leading and trailing strut arms are part of the standard design. For high-speed single-arm drogues, a small attachment lever arm is fitted near the leading edge of the canopy to enable control. Through manipulations of portions of the paradrogue material, forces perpendicular to the airflow can be generated that may be used to adjust the drogue position relative to the tanker or receiver aircraft. It is even conceivable that the drogue could detect a receiver approaching at a rate or angle that will result in a miss and either make corrections or maneuver away from the receiver, alerting the pilot using visual cues or wireless communication.

Although other concepts for drogue control exist, canopy manipulation is seen as advantageous because it builds on existing drogue architectures. The use of the existing canopy as the primary means of control eliminates the need for extra control surfaces that might break

off, causing foreign-object damage of the receiver, or need to be retracted to be properly stored in the stowage tube. The mechanism developed for this paper would collapse into the refueling pod after the hose is retracted. It is possible to fit all electronics, power systems, and actuators within the refueling coupling so that the controllable drogue can be attached to any existing hose–drogue system without modification to the tanker.

Several significant challenges are addressed in this paper. First, an aerodynamic model of a controllable drogue is generated and parameterized using wind-tunnel data of a refueling drogue modified for canopy manipulation. From these data, a hose–drogue dynamic model is generated to assess the maximum lateral and vertical position offsets relative to the steady-state catenary position that a controllable drogue could achieve. Then an automatic control algorithm is developed using linear quadratic regulator theory. Using a simulation generated from wind-tunnel data, the authors demonstrate precise positioning in the presence of winds, receiver forebody effects, and disturbances using the regulator.

Both a production low-speed and a production high-speed drogue were tested within a wind tunnel. For each drogue, a cruciform configuration of manipulators was implemented that distorted one of the four control points around the circumference of the drogue. Tests were conducted by manipulating each of the four locations separately and then in combinations of each location. Each drogue was tested at multiple airspeeds within the range of actual flight conditions for that drogue. For the test, the drogue was mounted to a sting that measured the three-axis forces and moments acting on the drogue at the defined wind conditions. Measurements were recorded as the sting changed both angle of attack (AOA) and angle of sideslip (AOSS). In each case, the actuation position was held constant as the drogue was rotated through a sweep of angle-of-attack and sideslip angles. Using the data measured, an aerodynamic database was generated and analyzed for both the low-speed and high-speed drogue to relate manipulator position, angle of attack, and angle of sideslip to the measured lift, drag, side force, rolling moment, pitching moment, and yawing moment of the drogue. These results are presented in this paper. To the authors' knowledge, this test represents the first published characterization of the stability derivatives of a drogue in this manner and for the purposes of control.

The reduced wind-tunnel data showed linearity in most of the control parameters, and the authors deduced a linearized set of coefficients. From this linearized data set, a linear quadratic regulator (LQR) is developed that tracks a desired position behind the tanker or relative to the receiver as a function of the measured flight condition. In simulation, the LQR algorithm is shown to stabilize the drogue in the presence of a variety of disturbances, including wind gusts provided by the NASA Dryden Flight Research Center (DFRC) wind-gust model [1] and receiver forebody effects generated in a simulation by Vassberg et al. [2]. The relationship of the drogue bandwidth requirements to the ability to attenuate disturbances is discussed in this paper.

Previous research into characterization of the drogue has been limited. Knacke [3] discussed general design and implementation of parachute systems. In particular, Knacke discussed general stability properties for various paradrogue designs. Although Knacke does not discuss refueling drogues, the general forms presented can be extrapolated to understand how the refueling drogue design provides natural stability at angles of attack or sideslip greater than 1 deg, and how the system has small instabilities resulting in rapid oscillations for angles of less than 1 deg. Both of these properties are exhibited in the wind-tunnel data. However, the small instability was ultimately removed from the simplified linear model generated in this paper, since this instability is minor in magnitude and effect relative to the control authority in the drogue control system presented.

Considerable research has been established on simulating tethered bodies as well as applications to refueling drogues. Eichler [4] developed a first-order perturbation solution for estimating the catenary angle and dynamic response of the hose, which did not require numerical integration or finite element methods. Characterizing the modulus of elasticity and the aerodynamic lift and drag of the hose, but using a simple drag model for the drogue, Eichler reported hose resonance frequencies in the range of 1.0–2.8 Hz. He analyzed tanker wing disturbances and found that these did not significantly affect drogue motion: in part, because the natural frequency of the hose was outside the amplification band of the wing vibrations. According to Eichler, the most significant effect came from wind-gust disturbances. The implication is that small tanker motion is not a relevant disturbance to the drogue stability problem.

Numerous other researchers have developed finite element methods for hose dynamics and investigated disturbances on those models. Zhu and Meguid [5] produced a finite element method and examined the effects of tanker disturbances and vortex wake behind the refueling pod. Their analysis indicates that a prime cause of drogue slap as the drogue is retracted may be vortex shedding on the refueling pod. Zhu and Meguid also demonstrated large disturbances from receiver coupling with the drogue causing a whipping effect on the hose. Similar results are predicted by Ribbens et al. [6] using another finite element method, although a simple technique of tension control is demonstrated that effectively eliminates the hose whipping action. The control method only measures the tension in the hose and requires no knowledge of the drogue/receiver coupling.

Vassberg et al. [2] showed significant simulation results of the drogue/receiver aerodynamic interaction. In this study, the hose was modeled using finite element methods with aerodynamics. The drogue was a rigid body. The flowfield around an F-18 aircraft with refueling probe extended was modeled. The results showed that the F-18 flowfield generated significant aerodynamic forces on the drogue, making more complex maneuvers necessary for commanding the receiver to couple with the drogue. Vassberg et al. contributed the F-18 flowfield used in this report, although it is noted that the flowfield was scaled for the lower airspeeds presented.

To the present knowledge of the authors, only limited efforts have been made to numerically characterize the drogue design parameters or stability derivatives before this study. Ro and Basaran [7] built scale models of the drogue and characterized the drag coefficient in the wind tunnel. Effects of the amount of fabric material and spacing of gaps in the canopy on drag coefficient were measured in the wind tunnel and compared with a computational fluid dynamics code. Although the results showed that the CFD code could predict trends in the drag coefficient, the results stopped short of attempting to characterize drogue stability derivatives or examine control authority.

The authors are aware of research[††] that provided an initial characterization of the side force generated by canopy manipulation concept in a wind-tunnel test at Texas A&M University. The results showed that the methodology using a high-speed drogue could generate 36 lbf of side force at 170 KIAS (knots indicated air speed) and predicted 76 lbf at 250 KIAS. These results demonstrated initial feasibility of the concept, but did not produce a full set of stability derivatives for the drogue or a six-degree-of-freedom aerodynamic model, nor did they characterize the variation in control authority discovered as a function of gravity. Interestingly, the results did verify the instability range for the drogue defined in Knacke [3] as ± 1.0 deg, which defines the region in which drogue angle of sideslip actually induces a rotational moment in the direction of the angle of sideslip. Outside of this region, an angle of sideslip induces a restoring moment to force the drogue back into alignment with the airflow.

A flight test was conducted in 1978 and reported by Elsworth et al. [8], in which a drogue with controllable surfaces that replaced the drogue canopy was deployed behind a CC-137. The drogue was radio-controlled from the receiver aircraft. The design was not actually a paradrogue. The paradrogue was replaced with control surfaces deflecting airflow to provide stability and control. The results of this nonparadrogue design showed poor controllability performance due to unpredicted and unmodeled effects. One important effect was the need to maintain constant drag to maintain altitude, requiring that every control action be countered by another action necessary to maintain constant drag.

One attempt to characterize the drogue and hose dynamics together was generated by Hansen et al. [9] at DRFC. In these

[††]Private communication with S. M. Stecko, D. A. Pruzan, and D. J. Lesieutre, 2006.

experiments, an F-18 aircraft with a buddy-store drogue system was flown with a receiver F-18 aircraft. Flying alone, the tanker F-18 pilot introduced pitching and yawing moment commands into the aircraft while the drogue was deployed. In addition, the receiver F-18 aircraft maneuvered behind the drogue to generate measurable bow–wake interactions. The results of these tests were characterizations of the frequency response of the hose that were significantly lower than those predicted by either Eichler [4] or Zhu and Meguid [5]. In addition, the results showed that the primary modes could be described with a second-order damped-oscillator function.

Based on these results, controllability tests were limited to examining stability in the presence of wind gusts and receiver forebody effects. The drogue slap was not addressed. A simple pendulum model was selected for simulation in which the hose is modeled as a rigid body, which is consistent with the results in Hansen et al. [9]. In this way, the results focus on the primary work in this paper: the characterization of the drogue aerodynamics and ability to manipulate these dynamics to produce significant forces that can be used for stability and control. Clearly, more sophisticated hose models will generate different results. However, within the bounds of the real-time flight tests of Hansen et al. and the frequency response predicted by Zhu and Meguid [5], the assumption of a second-order system is reasonable for this initial study of the hose and drogue interaction.

This paper is broken down into several sections. Section II discusses the wind-tunnel test, methodology, and data collected. Section III discusses the model developed as a result of this wind-tunnel test and includes the dynamics of the hose pendulum model. An LQR control system is developed in Sec. IV for either stability or control. Simulation results demonstrating the controllability of the drogue are presented in Sec. V. These results show controllable response to wind gusts, receiver forebody effects, and the effect of actuator lag.

II. Wind-Tunnel Test Results

Three wind-tunnel tests were conducted during this program to characterize the aerodynamic performance of existing drogues. Tests were completed at the Wichita State University (WSU) National Institute for Aviation Research wind tunnel. The first two wind-tunnel tests were conducted using the C-130 low-speed drogue in February and April 2008. The low-speed drogue typically produces 300–800 lb of drag at airspeeds between 90 and 130 KIAS. The third wind-tunnel test was carried out using the 767 wing aerial refueling pod high-speed drogue. This test was conducted to determine if the concept used for the low-speed drogue could be transferred to the high-speed drogue. Only the low-speed drogue is described, although similar results were achieved with the high-speed drogue.

The production C-130 low-speed drogue has a standard drogue coupling. The low-speed drogue used a standard straight-line coupling shroud that could fit into the Sergeant Fletcher stowage tube. The shroud tapers from 8.5 to 10 in. in diameter. The drogue canopy is attached to the coupling using an outer ring of 18 leading-edge strut arms that connect to the outer edge of the canopy and 36 trailing-edge strut arms that connect to the inner ring of the single-lobe canopy. The term *leading edge* is used to refer to the outer ring of struts, because these struts are farther forward in the air flowfield than the inner-ring, or trailing-edge, struts. Two additional leading-edge struts were added to the basket to accommodate a cruciform-type modulation for a total of 20 evenly spaced leading-edge struts. Eight leading-edge and eight trailing-edge strut arms were modified to permit manipulation of the canopy by expanding and contacting the angle between the leading and trailing strut arms. Rigid strut braces were used to hold the leading- and trailing-edge strut arms at a fixed angle of separation. Two strut braces were used per quadrant of the drogue for a total of eight. The strut locations on the drogue are referred to as the starboard brace (actuator 1), the port-side braces (actuator 3), the upper brace (actuator 2) aligned with the vertical, and the lower brace (actuator 4) aligned with the vertical. The strut braces had numbered separator positions. Table 1 shows the correlation between the strut-brace position used in the wind-tunnel tests and the separation angle between the leading-edge strut and its corresponding trailing-edge strut.

Table 1 strut-brace position and strut-arm separation angle

Strut position	Separation angle, deg
1	50.03
2	47.71
3	45.20
4	42.45
5	40.15
6	37.62
7	35.13
8	32.72
9	30.24
10	27.77
11	25.37
12	23.00

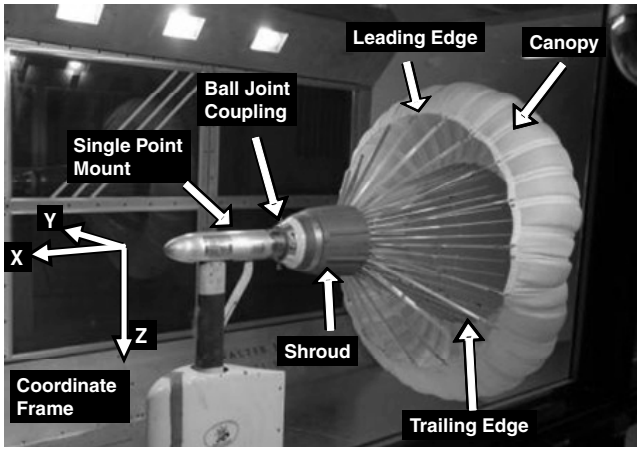

Fig. 1 Wind-tunnel test configuration.

Figure 1 shows the wind-tunnel test-section setup with a fully inflated drogue attached to the single-point mount. The drogue canopy, the leading edge of the canopy, and the trailing edge of the canopy are all defined. The drogue shroud covers the drogue MA-3 refueling coupling. The ball-joint coupling connects the drogue to a refueling hose and was also used to connect the drogue to the wind-tunnel sting. A wind-tunnel brace was manufactured to hold the drogue coupling at a fixed AOA/AOSS and to act as an interface for the wind-tunnel single-point mount and the low-speed drogue. The brace restricted motion of the drogue ball joint vertically and laterally, but did not restrict roll so that the drogue could be rotated for different portions of the test. The roll angle was checked multiple times between tests using a digital level and did not change to within the 0.1 deg precision of the instrument, unless manually moved. The single-point mount was bolted to the WSU Walter Beach low-speed wind-tunnel external balance. The forces and moments were measured from the wind tunnel's external balance and translated to the point at which the drogue coupling interfaced with the wind-tunnel mount. The drogue coordinate frame was defined using standard aircraft coordinates, such that the drogue coupling to the sting was designated the front of the vehicle. The positive X axis passed through the center of the drogue toward the oncoming wind. The Y axis pointed starboard, and the Z axis pointed down. The forces included lift force (vertical in the wind tunnel), side force (starboard in the drogue body frame), and drag force (along the X axis). Pitching moment was about the Y axis, yawing moment was about the Z axis, and rolling moment was about the X axis.

Wind-tunnel data collected consists of the measured forces and moments acting at the point at which the drogue coupling attaches to the wind-tunnel mount. The single-point mount could be commanded to hold an angle of attack or angle of sideslip relative to the wind tunnel. Data for the low-speed drogue were taken at a fixed airspeed of 115 KIAS, which was later corrected for blockage effects

and estimated to be 125 KIAS, near the top limit for this drogue. The test plan was designed to isolate the effect of each strut brace and then show how different combinations of strut braces affected the measured forces and moments. The AOSS profiles varied from −10 to +10 deg in 1 or 2 deg increments. The AOA was varied from 0 to +5 deg in 1 deg increments. The port and starboard strut braces were assumed to generate a symmetric forces. Several test points were used to verify this claim. Symmetry was not assumed between the upper and lower braces, since drogue shape was clearly distorted due to gravity, even at 125 KIAS. Other test points provided combinations of symmetric or asymmetric deflections of combinations of strut-brace locations to assess actuator control symmetry and independence.

The procedure consisted of manually setting the desired strut-brace angle. Then the wind tunnel was started and given time to settle. The sting was automatically rotated through the desired sweep of AOA or AOSS, stopping for at least 10 s after each move to let the wind tunnel settle. Force and moment data were collected, filtered, and averaged over an additional 10 s at each AOA and AOSS. These forces and moments along with measurements of the dynamic pressure in the freestream of the wind tunnel were used to generate force and moment coefficients normalized to a 1 ft^2 reference area and 1 ft lever arm.

A. Aerodynamic-Data-Table Fits

Data tables and curve fits were used to reduce the data into a format for analysis and simulation. The data tables used the strut-brace hole position, drogue angle of attack, and sideslip as inputs to generate the linearly interpolated force and moment coefficients. Angle of attack is valid from 0 to 5 deg and is interpolated beyond these points. Angle of sideslip is valid from −10 to 10 deg and is interpolated outside of that region.

The broad range of data and multiple dependencies force the analyst to examine only the relevant interdependencies in three-dimensional plots. Of importance is the inherent assumption that the drogue is symmetric about the vertical axis. Therefore, it is assumed that force and moments generated by actuator 3 (port) are equal and opposite to the forces and moments generated by actuator 1 (starboard). Unless specified, all actuators are assumed to be at a fixed-hole location at hole 9 (30.24 deg of separation between leading and trailing edge).

Figure 2 shows the lateral control results. The left plot shows side-force coefficient as a function of actuator 3 (port-side) position and angle of sideslip. In this plot, a low strut position number generates a positive side force in the direction of the actuator. A high strut position (greater than 9) can actually generate a force in the opposite direction. The increase in angle of sideslip (front of drogue to starboard) generates a side-force coefficient that pushes the drogue to starboard. The results are largely linear with both angle of attack and strut-angle position. The figure on the right shows that side force is nearly linear with angle of sideslip and that the angle of attack has almost no influence on side force, indicating that a cruciform control configuration may decouple lateral and longitudinal control.

Figure 3 shows longitudinal control results. The left plot shows the lift coefficient (positive down) as a function of angle of attack and actuator 2 (top). As angle of attack increases, the drogue generates more lift. In this case, the positive angle of attack increases the

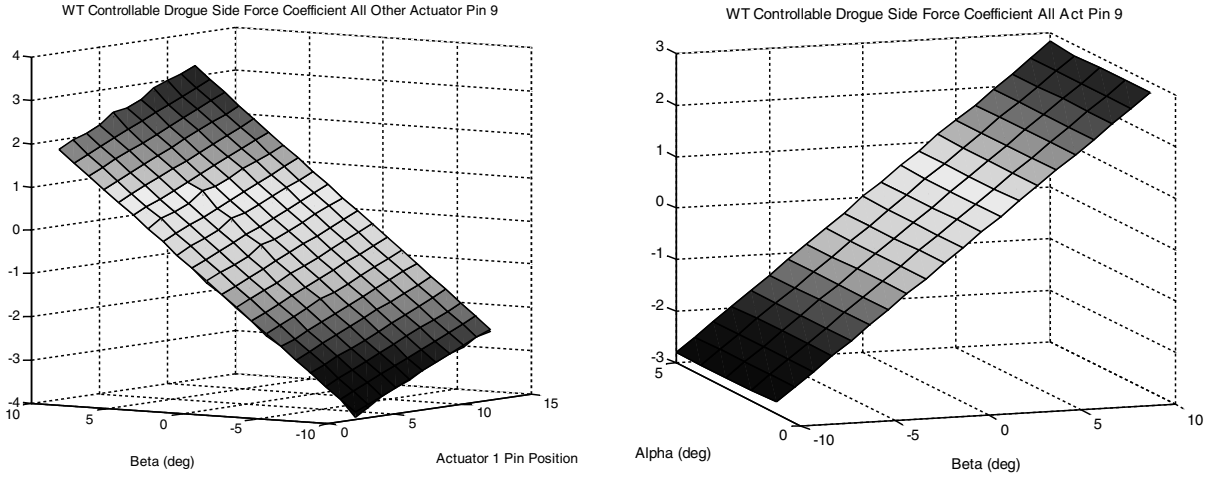

Fig. 2 Side-force coefficient as a function of beta and actuator 1 and alpha and beta (right);WT denotes wind tunnel.

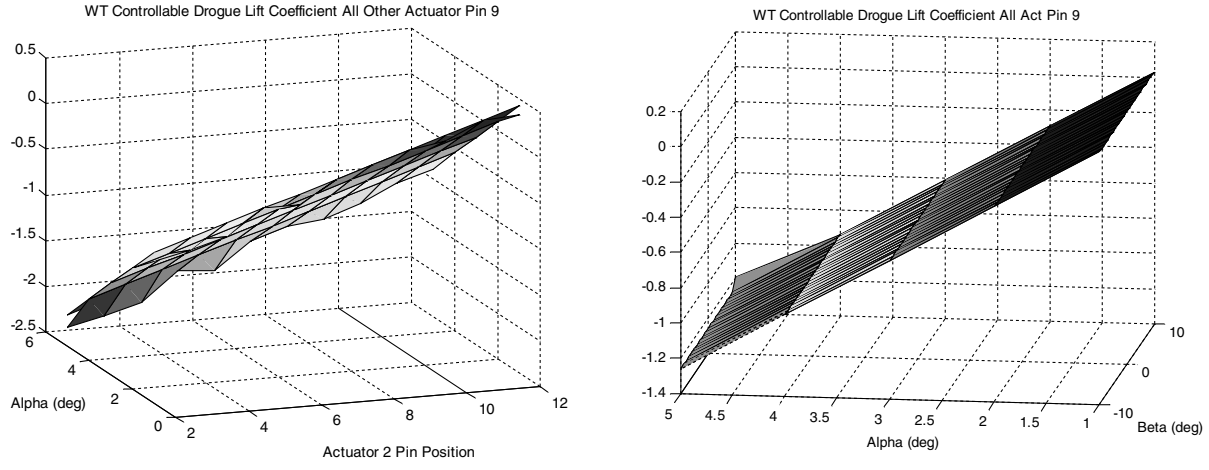

Fig. 3 Lift-force coefficient as a function of alpha and actuator 2 (left) and alpha and beta (right).

control effectiveness of actuator 2 so that the actuator generates more lift at high angle of attack. The second plot shows that lift is nearly linear with angle of attack and has almost no relationship to angle of sideslip.

Drag coefficients are depicted in Fig. 4. On the left, drag coefficient is a function of both angle of sideslip and actuator position. The local maximum occurs at zero sideslip and position 6 for actuator 1. In fact, the maximum drag is achieved when all actuators are at position 6. The right-hand plot shows the relationship of angle of attack and sideslip. The plot shows the decrease in drag with respect to angle of attack. However, it is noted that negative angle of attack was not tested, and it is assumed that drag would decrease as angle of attack decreased. The trim point of maximum drag with respect to angle of attack is not at zero and is estimated using the numerical methods presented in the next section.

Pitching-moment coefficients are depicted in Fig. 5. The left plot shows a strong linear correlation between the pitching moment and actuator 2. Weak correlation is also displayed for actuator 1, although significantly less than for actuator 2. The data show that actuator 1 can induce a rotational motion to rotate the drogue nose-down. The right-hand plot shows the nearly planar relationship of actuator 2 and angle of attack.

Yawing moment is depicted in Fig. 6. The right plot shows a very linear relationship with actuator 1 and no effect of actuator 2. The right-hand plot shows that angle of sideslip dominates yawing moment, but actuator 1 does have a linear effect. As actuator 1 position decreases, generating a negative side force, it also generates a positive yawing moment, which acts against the restoring moment of the actuator position.

Rolling moment was measured during the tests. The data showed a positive bias regardless of the configuration of actuators, angle of attack, or sideslip. However, less rolling moment was observed than actuator 2 generated pitching moment by a factor of 30 peak to peak after the rolling moment bias was removed. The numerical fit presented in the next section takes into account the rolling moment and weak effects observed due to actuator position. During the test, the coupling between the drogue and the mount was free to rotate in roll. A digital level was used to measure the roll angle between tests and showed no rotation. The rolling moment, although weakly present, was not enough to overcome the friction on the drogue coupling. Clearly, rolling moment may exist in flight: especially in an asymmetric or damaged drogue. It may be that a relatively new ball joint was used and an older, more worn, ball joint might have less friction, which would allow the drogue to roll. However, initial results indicated that a weak rolling moment was induced even with asymmetric actuator commands. The rolling moment will need to be dealt with either through control or instrumentation means.

B. Comparisons of Actuator Effectiveness

At zero angle of attack and sideslip, the maximum lift coefficient for actuator 2 changed from approximately 0.6 at the minimum actuator setting to −0.6 at the maximum actuator setting, and the maximum side-force coefficient for actuator 1 changes from 0.2 to 1.2. The effective slope for actuator 1 is approximately 0.1 coefficient points per actuator position, and the effective slope for actuator 2 is 0.12 coefficient points per actuator position. Actuator 2 seemed to generate lift in both directions, whereas the bias heavily skewed actuator 1 to generate forces only in one direction. However, the slope of actuator 4 was 10.5% less than for actuator 2. Further, the intercept for actuator 2 is 0.65, and the intercept for actuator 4 was −1.32 in coefficient counts.

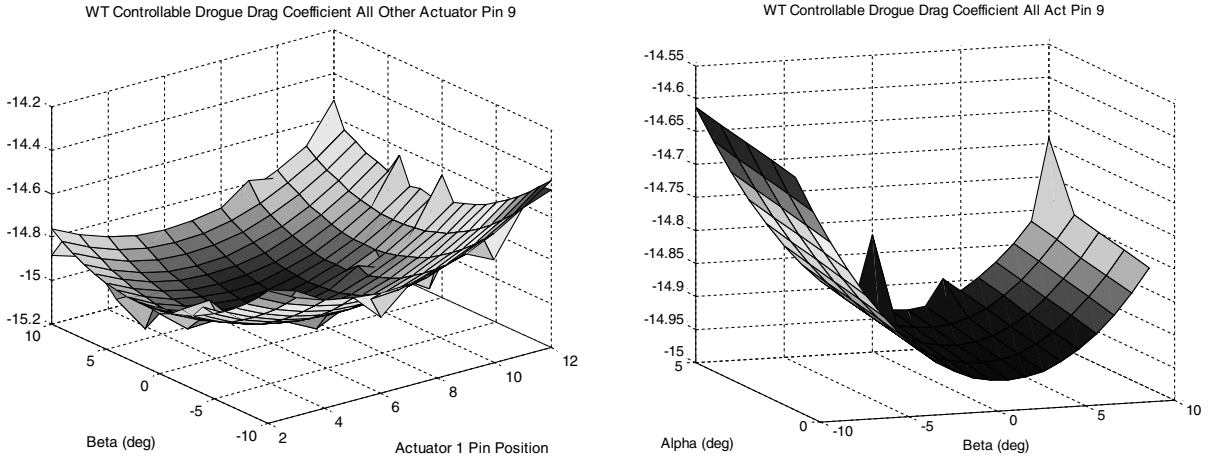

Fig. 4 Drag coefficient as a function of beta and actuator 1 (left) as well as alpha and beta (right).

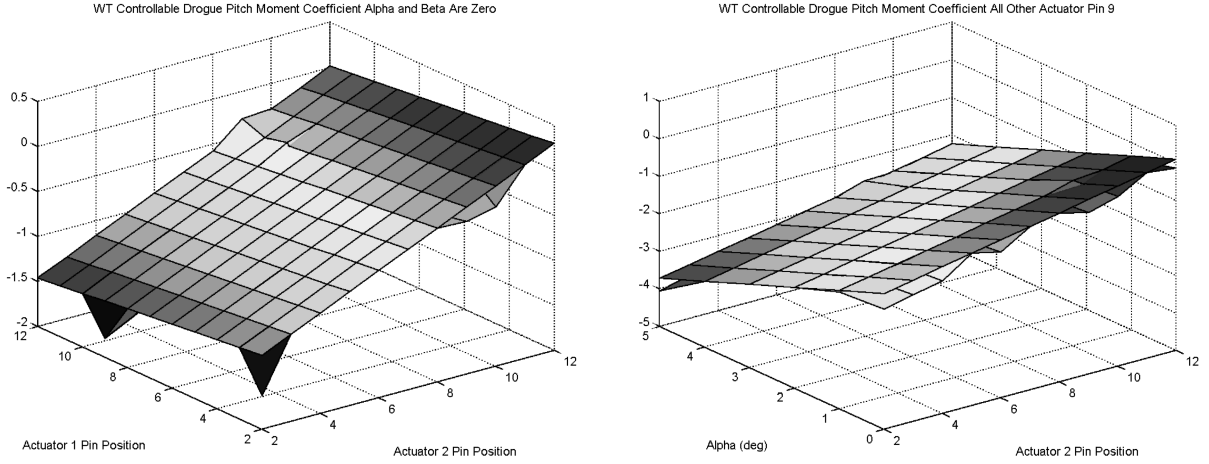

Fig. 5 Pitching moment as a function of actuator 1 and 2 (left) and actuator 2 and alpha (right).

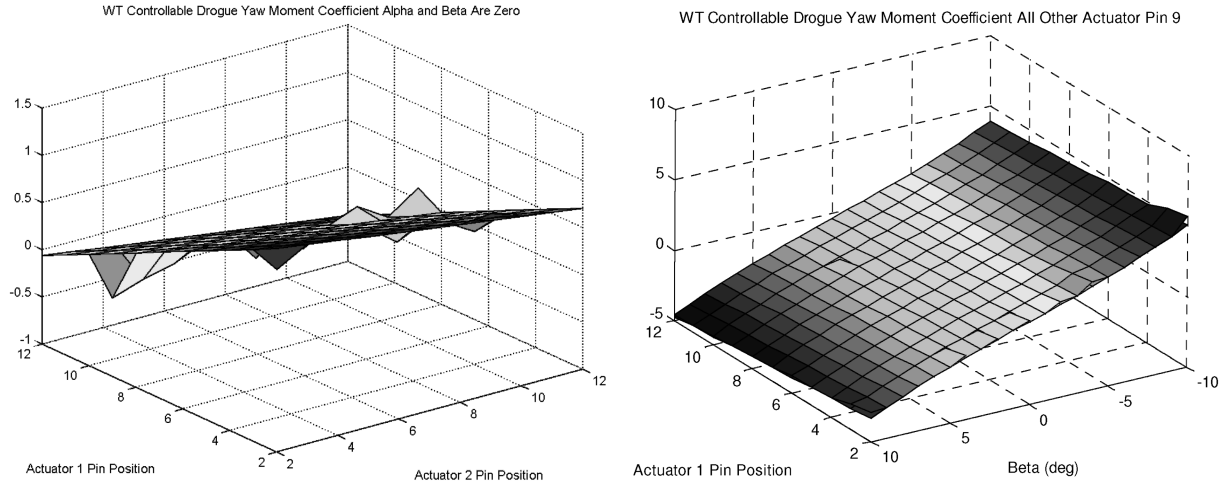

Fig. 6 Yawing moment as a function of actuator 1 and 2 (left) and actuator 1 and beta (right).

Three possible causes for the difference have been examined. First, manufacturing defects may exist. However, these have been ruled out by rotating the drogue a full 90 deg and seeing that the lift force generated by actuator 1 matches the lift force generated by actuator 2 when in the same configuration. Manufacturing differences in strut arms resulted in variations of 10% or less in lift and side force generated at each position. Second, the wind tunnel itself could be generating the effect. The wind tunnel is a 7 ft vertical by 10 ft horizontal wind tunnel. The upper tip and lower tip of the drogue are within 1.5 ft of the ceiling and floor. The sting is directly in front of actuator 4, which may contribute to changes in the flowfield around actuator 4. The most likely cause is that gravity is distorting the shape of the drogue by causing actuator 4 to sag relative to actuator 2.

The drogue was rotated in the wind tunnel so that the actuators were placed at a 45 deg angle from the baseline condition. The lift and side forces were predictably intermediate between what was generated at either a 0 or 90 deg location. The relationship was nonlinear, but symmetric about the vertical axes. The results for actuators 2 and 4 in the 45 deg position indicated a smooth transition in force coefficient from the vertical to horizontal position. This result would seem to indicate that gravity distortion of the drogue strut-arm shape plays a dominant role in the difference in performance of the top and bottom actuators.

In summary, the results show that actuators on either side of the horizontal axis will have the same control authority with small variation. Actuators on the top of the drogue will have significantly different authority from those on the horizontal axis or those on the bottom of the drogue. As the drogue rolls, the amount of control authority of each actuator will change. However, the results show that the amount of change is gradual as a function of roll angle and can be predictable. More data points are required to provide an adequate curve fit to predict the change in force generated by a particular actuator as a function of the roll angle of the drogue relative to gravity or the local horizontal in future tests.

C. Comparisons of Number of Strut Arms

Tests were conducted in which one, two, and three strut arms were used to actuate the canopy for each quadrant. The results presented in the previous sections all assumed two strut arms per quadrant, which translates to 10% of the circumference of the canopy deflected at each actuator location. Tests were conducted using only one strut arm (5% canopy area deflection) and again for three strut arms (15% canopy area deflection). In all three cases, the actuator position was set to position 2 (50 deg). The results showed that a single strut arm produced only 68% of the side force of the two strut-arm actuator at maximum deflection. Three arms produced 38% more side force than two strut arms. The amount of increase is not linear, but does indicate that adding a third strut arm does significantly increase the side force generated per actuator.

D. Actuator Mechanism Design

Load cells were placed on one of the strut arms located at actuator position 1 to measure the amount of tension or compression in the arm. The load cell data were largely linear with respect to separation angle. The maximum compression measured was approximately 60 lbf. The maximum tension was 15 lbf. The amount of compression or tension on actuator 1 was not significantly different when the actuator was rotated to the vertical position (actuator 2). The neutral position where there was no force on the struts was located between positions 9 and 10. Data recorded showed that strut tension was nearly constant over the range of AOA tested for all actuators. Data showed a 5 lb variation from -10 to 10 deg of AOSS on the lateral actuators and about a 2 lb variation on the vertical actuators from 0 to 5 deg of AOA at maximum deflection. This variation sets the limits for how much additional force is required to hold a strut-angle position at various AOSS and AOAA. Since two struts were used in this test, it is surmised that a total of 120 lb of force is required to separate the leading- and trailing-edge struts in each quadrant when using two struts per quadrant.

A mechanical actuator system was designed and analyzed to determine the power requirements for operating this type of control system on the drogue. The mechanism consists of a set of linkages controlled by a cable attached to a servo motor. Given the forces at each angle of separation between the strut arms and the mechanism designed, the mechanism proposed could force the full separation between the strut arms using only a few inches of cable travel. From these values of force and travel, as well as the response rate limits of 10, 25, and 50 deg/s on the separation of the strut arms, it was possible to calculate the instantaneous power requirements. A conservative estimate of power requirements for the 10, 25, and 50 deg/s was 14.0, 34.0, and 68.0 W, respectively. If it can be shown that the control bandwidth requirements can operate under a variety of conditions and require only a minimum angular rate for stability, then the power system on the controllable drogue may be self-contained using batteries or wind generation, as appropriate. The lower the angular rate, the less power is required to operate the controllable drogue. Therefore, lower rate limits are desirable.

III. Simulation and Control Model

A numerical model of the drogue was generated for a simulation. Parameter estimation was used to reduce the aerodynamic data into functional form. Hose dynamics were modeled as a two-arm pendulum. The simulation was used to define the maximum achievable catenary position relative to the tanker. Using the estimated parameters, a control law was developed and tested against a variety of disturbances, including receiver forebody effects and wind gusts.

A. Aerodynamic-Data Fit

A linearized aerodynamic model was fit to the wind-tunnel data. The aerodynamics were modeled as shown in Eq. (1). In this case,

$$C_0 = [\,C_{D0} \quad C_{Y0} \quad C_{L0} \quad C_{rm0} \quad C_{pm0} \quad C_{ym0}\,]^T$$

is the baseline 6-element vector containing the bias values for the drogue,

$$C_u = [\,C_{u1} \quad C_{u2} \quad C_{u3} \quad C_{u4}\,]$$

is a 6 by 4 element matrix containing the forces and moments parameters for each of the four actuators with

$$C_{ui} = [\,C_{Dui} \quad C_{Yui} \quad C_{Lui} \quad C_{rmui} \quad C_{pmui} \quad C_{ymui}\,]^T$$

for actuator i. The vector u_{act} is the 4 by 1 vector of the actuator positions, u_0 is the position about which the system is linearized (position 9),

$$C_\alpha = [\,C_{D\alpha} \quad C_{Y\alpha} \quad C_{L\alpha} \quad C_{rm\alpha} \quad C_{pm\alpha} \quad C_{ym\alpha}\,]^T$$

is the 6 by 1 vector of force and moment sensitivities to angle of attack α, and

$$C_\beta = [\,C_{D\beta} \quad C_{Y\beta} \quad C_{L\beta} \quad C_{rm\beta} \quad C_{pm\beta} \quad C_{ym\beta}\,]^T$$

is the 6 by 1 vector of force and moment sensitivities to angle of sideslip β. The trim angle of attack α_0 was set to 2.0 deg based on running steady-state simulations and noting that the drogue tends to trim at 2.0 deg of angle of attack:

$$\begin{bmatrix} F^{Bd}_{\text{aero}} \\ M^{Bd}_{\text{aero}} \end{bmatrix} = \bar{q} f(u_{\text{act}}, \alpha, \beta) \approx \bar{q}\left(C_0 + C_u(u_{\text{act}} - u_0) + [\,C_\alpha \quad C_\beta\,]\begin{bmatrix} \alpha - \alpha_0 \\ \beta \end{bmatrix}\right) \tag{1}$$

Values were fit to all 42 of the parameters described using a least-squares methodology to solving the formula:

$$A_{6N\times 42} x_{42\times 1} = b_{6N\times 1} \tag{2}$$

In this case, N was the total number of data points. The vector b contains the three forces and three moments for each of the N runs. The vector x is defined as shown in Eq. (3), and one column of the sensitivity matrix A is defined in Eq. (4), where A_i is an index on the run number with $i = 1$ to N:

Table 2 Base coefficients for low-speed drogue

Coefficients	Values	Units
C_{D0}	27.8844	ft^2
C_{Y0}	0.0000	ft^2
C_{L0}	−0.3012	ft^2
C_{rm0}	0.0000	in. · ft^2
C_{pm0}	−1.2842	in. · ft^2
C_{ym0}	0.0000	in. · ft^2

$$x = \begin{bmatrix} C_0 \\ C_{u1} \\ C_{u2} \\ C_{u3} \\ C_{u4} \\ C_\alpha \\ C_\beta \end{bmatrix} \tag{3}$$

$$A_i = \begin{bmatrix} I_{6\times 6} \\ A_{\alpha i} \\ A_{\beta i} \\ I_{6\times 6}(u_1 - u_0) \\ I_{6\times 6}(u_2 - u_0) \\ I_{6\times 6}(u_3 - u_0) \\ I_{6\times 6}(u_4 - u_0) \end{bmatrix} \tag{4}$$

The angle-of-attack and sideslip drag coefficients were tuned to a function of the cosine of angle of attack and sideslip, and the other terms were considered linear with respect to angle:

$$A_{\alpha i} = \begin{bmatrix} \cos(\alpha-\alpha_0) & 0 & 0 & 0 & 0 & 0 \\ 0 & (\alpha-\alpha_0) & 0 & 0 & 0 & 0 \\ 0 & 0 & (\alpha-\alpha_0) & 0 & 0 & 0 \\ 0 & 0 & 0 & (\alpha-\alpha_0) & 0 & 0 \\ 0 & 0 & 0 & 0 & (\alpha-\alpha_0) & 0 \\ 0 & 0 & 0 & 0 & 0 & (\alpha-\alpha_0) \end{bmatrix} \tag{5}$$

$$A_{\beta i} = \begin{bmatrix} \cos(\beta) & 0 & 0 & 0 & 0 & 0 \\ 0 & \beta & 0 & 0 & 0 & 0 \\ 0 & 0 & \beta & 0 & 0 & 0 \\ 0 & 0 & 0 & \beta & 0 & 0 \\ 0 & 0 & 0 & 0 & \beta & 0 \\ 0 & 0 & 0 & 0 & 0 & \beta \end{bmatrix} \tag{6}$$

Although the actual wind-tunnel data only measured the performance of actuators 1, 2, and 4 directly, actuator 3 (port-side actuator) was assumed to have the same performance as actuator 1. This assumption was validated by collecting a few test points during the tests for actuator 3. To complete the data set, all data corresponding to variations in actuator 1 were reflected about the drogue X–Z plane to simulate equal but opposite forces for actuator 3. Although it is noted that actuator effectiveness changes as a function of roll angle, this analysis did not use any of the data in which the drogue was rotated at 45 deg relative to the standard position Total control authority is not expected to change with roll angle, merely how a control law would be required to respond given a particular roll orientation. However, as noted before, future work should include the effect of roll on actuator performance by adding more test points to the wind-tunnel data:

$$x = (A^T A)^{-1} A^T b \tag{7}$$

A least-squares estimator was constructed to provide the solution as shown in Eq. (7). The results are presented in Tables 2–5. Note that in the tables for angle of attack and sideslip, the units of the drag

Table 3 Actuator coefficients for low-speed drogue

Coefficients	$u1$	$u2$	$u3$	$u4$	Units
C_{Dui}	−0.0093	−0.0112	−0.0093	−0.0037	ft^2/actuator deg
C_{Yui}	−0.0607	0.0000	0.0607	0.0000	ft^2/actuator deg
C_{Lui}	−0.0037	−0.0575	−0.0037	0.0570	ft^2/actuator deg
C_{rmui}	0.0069	0.0000	−0.0069	0.0000	in. · ft^2/actuator deg
C_{pmui}	−0.0013	−0.0727	−0.0013	0.0695	in. · ft^2/actuator deg
C_{Ymui}	0.0644	0.0000	−0.0644	0.0000	in. · ft^2/actuator deg

Table 4 Angle-of-attack coefficients

Coefficients	Values	Units
$C_{D\alpha}$	−30.3174	ft^2/ deg
$C_{Y\alpha}$	0.0000	ft^2/ deg
$C_{L\alpha}$	−0.3106	ft^2/ deg
$C_{rm\alpha}$	0.0000	in. · ft^2/deg
$C_{pm\alpha}$	−0.4744	in. · ft^2/deg
$C_{ym\alpha}$	0.0000	in. · ft^2/deg

Table 5 Angle-of-sideslip coefficients

Coefficients	Values	Units
$C_{D\beta}$	−12.3570	ft^2/ deg
$C_{Y\beta}$	0.2830	ft^2/ deg
$C_{L\beta}$	0.0000	ft^2/ deg
$C_{rm\beta}$	0.0035	in. · ft^2/deg
$C_{pm\beta}$	0.0000	in. · ft^2/deg
$C_{ym\beta}$	−0.4202	in. · ft^2/deg

coefficient are relative to radians, since that particular coefficient is multiplied by the cosine of angle of attack or sideslip rather than the actual angle of attack or sideslip.

The predicted forces and moments generated using the linearization are in good agreement with the actual data to within about 5% on drag, side force, lift, and yawing moment. Pitching moment is a bit worse at 15% at the extreme actuator and angle-of-attack positions. The roll signal, as discussed previously, is extremely weak and its impact on simulation is minimal.

B. Kinematic Model

The wind-tunnel data were used to update the aerodynamic database and input into the nonlinear simulation developed for the purposes of evaluating the six-degree-of-freedom system using a control law to stabilize the drogue. The initial model developed consists of a simple pendulum consisting of the pendulum lever representing the hose and the drogue aerodynamic model. The model is displayed in Fig. 7 in two dimensions, although the simulation includes all three linear and all three rotational degrees of freedom.

In Fig. 7, a rigid lever is mounted to a fixed point in inertial space through an assumed ball joint. The pendulum is free to rotate about any axis, but is pinned to that point in space. The fixed point is constrained from moving, regardless of the force exerted by the lever. The lever has mass and gravity acts on the lever. Aerodynamic forces act at the center of gravity based on the coefficients developed by Eichler [4].

At the other end of the lever is the drogue attached to the lever through a second ball joint. The drogue model includes mass properties, rotational inertia, and aerodynamic properties. The mass and moment of inertia of the drogue are calculated using mass

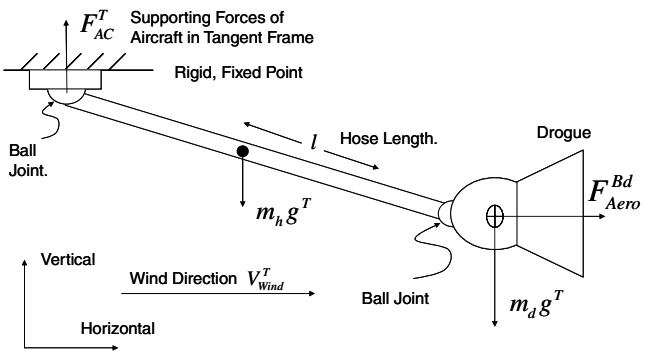

Fig. 7 Drogue dynamic pendulum model.

Table 6 Hose mass properties

Hose dimensions	Value	Unit
Length	100	ft
Radius	3.37	in.
Empty density	2.25	lb/ft
Fuel density	2.215	lb/ft

Table 7 Drogue mass properties

Drogue dimensions	Value	Unit
Shroud weight	50	lbs.
Shroud length	16	in.
Shroud radius	5.25	in.
Trailing-edge strut weight	6.2	oz
Trailing-edge strut length	275	in.
Trailing-edge strut radius	0.25	in.
Total trailing-edge struts	36	Struts
Leading-edge strut weight	4.9	oz
Leading-edge strut length	21	in.
Leading-edge strut radius	0.25	in.
Total leading-edge struts	20	Struts
Number of leading-edge controls struts	2	Struts
Total assumed X c.g. location	18.5	in.

properties of the drogue shroud and canopy struts. The canopy fabric is assumed to be without mass. Gravity acts on the drogue center of gravity calculated from the model, and the rotational moment of inertia is calculated at the ball joint. The aerodynamic-data table or linearized coefficient model discussed previously generates the associated forces and moments that the drogue canopy experiences as a function of airspeed, angle of attack, angle of sideslip, and actuator position. The forces were translated from the wind-tunnel sting to the center of gravity for the simulation. The moments were translated from the sting to the ball-joint coupling.

A constant wind gust simulating flight speeds passes over the drogue. The weight of the lever arm and drogue balances the aerodynamic drag generated by the drogue, which results in a steady-state catenary angle of the lever arm relative to the horizontal axis. The DFRC wind-turbulence model is added to the steady-state wind to simulate the effects of gusts.

The relevant mass properties used in the simulation are presented in Tables 6 and 7. The hose inertia was modeled as a long, thin cylinder. The drogue shroud and coupling were modeled as a single cylinder. Each strut arm was modeled separately as a long, thin cylinder. The trailing-edge struts were assumed to be fixed, and the leading-edge struts moved with the commanded angle. However, the effect of this type of modeling on rotational inertia was insignificant, since most of the mass was in the drogue coupling. Simulation results were conducted assuming that the hose was full of fuel. The center of gravity of the drogue was assumed to be on the centerline of the drogue.

Because the system is described as pendulum with two bars, the nonlinear equations of motion may be defined using only 12 states: three attitudes for the hose and associated three angular rates and then three attitudes of the drogue and associated three angular rates. This simplification ignores the effect of the tanker forces acting at the interface between the hose and drogue, but is sufficient for studying the effect of disturbances on the drogue of the hose–drogue system.

The force balance assumes that the connection at the aircraft is stationary so that the sum of all forces at that point is zero, as shown in Eq. (8). In this case, F_{AC}^{T} is the force vector of the aircraft (AC) acting in the local tangent frame T. The mass of the hose m_h and the mass of the drogue m_d are acted on by the force of gravity in the tangent frame g^T. The cosine rotation matrix C_{Bd}^{T} rotates the total forces acting on the drogue F_{aero}^{Bd} from the drogue body frame into the local tangent frame. The sum of moments acting at aircraft interface point M_{AC}^{Bl} are shown in Eq. (9) and the moments are equal to the forces acting on the hose crossed with the lever arm of action: in this case, either half or the full length of the beam l. The rotation matrix C_{Bl}^{T} rotates the hose body frame to the local tangent frame. The hose body frame has the

x axis along the length of the beam, the y axis is to starboard, and the z axis is down. Note that the positive x axis actually points forward toward the tanker. Note that an intermediate force F_d^{Bd} is introduced as the total force transmitted from the drogue to the lever arm through the ball-joint coupling represented in the drogue body frame. The moment M_F^{Bl} represents the friction moment transferred between the drogue and the hose coupling:

$$F_{\text{AC}}^T = m_h g^T + m_d g^T + C_{Bd}^T F_{\text{aero}}^{Bd} \tag{8}$$

$$M_{\text{AC}}^{Bl} = \tfrac{1}{2} l^{Bl} \times C_T^{Bl} m_h g^T - l^{Bl} \times C_T^{Bl} C_{Bd}^T F_d^{Bd} - C_T^{Bl} C_{Bd}^T M_F^{Bd} \tag{9}$$

The forces and moments acting at the hose–drogue ball-joint coupling are shown in Eqs. (10) and (11), respectively:

$$F_d^{Bd} = C_T^{Bd} m_d g^T + F_{\text{aero}}^{Bd} \tag{10}$$

$$M_d^{Bd} = L_{\text{CG}}^{Bd} \times C_T^{Bd} m_d g^T + M_{\text{aero}}^{Bd} + M_F^{Bd} \tag{11}$$

Calculating the friction moment between the hose and drogue ball-joint coupling is difficult, since the static friction coefficient is very large, which poses problems with numerical integration algorithms when the system switches quickly from static to dynamic friction. As a first attempt to estimate friction, a scale factor was applied to the angular velocity to act as a damping force. However, this method was seen as too optimistic, especially for control law design, because the static friction of the ball joint is large. When the transition is made from static to dynamic friction, the responsiveness of the drogue will radically change. Properties of the drogue were estimated from existing knowledge to implement this model. The radius of the ball joint r_{ball} was taken from drogue schematics to be 4.0 in., and the preload force F_{preload} was estimated as 300 lbf of drag on the drogue during flight. Using [10], values of the static and kinetic coefficients of friction were defined based on steel-on-steel contact as $\mu_S = 0.74$ and $\mu_K = 0.57$, respectively. Normal force on the ball joint was then calculated using the preload and friction coefficients. The normal force was used to generate a minimum static friction moment. If this moment was exceeded, then a transition to a dynamic coefficient occurred and the drogue was allowed to rotate relative to the hose. We note that this model is far from perfect, but is suitable for estimating the effect of a stiff ball joint, such as those used on the drogue, on overall stability.

The rotation matrix C_{Bl}^T defines the orientation of the hose lever arm relative to the local tangent and may be represented interchangeably with either Euler angles or a quaternion Q_{Bl}^T; the definitions of these transformations and other kinematic expressions may be found in Zipfel [11]. The time derivative of the lever-arm quaternion is depicted in Eq. (12), where the 4×4 matrix Ω_{TBl}^{Bl} is a special form of the angular velocity vector ω_{TBl}^{Bl}, as shown in Eq. (13). The 3×1 vector ω_{TBl}^{Bl} represents the angular velocity of the hose lever-arm body frame relative to the local tangent represented in the hose lever-arm body frame. The time derivative of the angular velocity ω_{TBl}^{Bl} at the tanker interface ball joint is given in Eq. (14), where the inertia tensor of the drogue lever arm is represented by I_{Bl} in the hose body frame. A similar set of kinematic equations of motion is defined for the drogue at the hose–drogue ball-joint coupling in Eqs. (15–17), with the drogue angular velocity defined as ω_{TBd}^{Bd} and the drogue moment of inertia defined by I_{Bd}:

$$\dot{Q}_{Bl}^T = \tfrac{1}{2} \Omega_{TBl}^{Bl} Q_{Bl}^T \tag{12}$$

$$\Omega_{TBl}^{Bl} = \begin{bmatrix} 0 & -\omega_x^{Bl} & -\omega_y^{Bl} & -\omega_z^{Bl} \\ \omega_x^{Bl} & 0 & -\omega_z^{Bl} & \omega_y^{Bl} \\ \omega_y^{Bl} & \omega_z^{Bl} & 0 & -\omega_x^{Bl} \\ \omega_z^{Bl} & -\omega_y^{Bl} & \omega_x^{Bl} & 0 \end{bmatrix}; \qquad \omega_{TBl}^{Bl} = \begin{bmatrix} \omega_x^{Bl} \\ \omega_y^{Bl} \\ \omega_z^{Bl} \end{bmatrix} \tag{13}$$

$$\dot{\omega}_{TBl}^{Bl} = I_{Bl}^{-1} (M_{\text{AC}}^{Bl} - [\omega_{TBl}^{Bl} \times] I_{Bl} \omega_{TBl}^{Bl}) \tag{14}$$

$$\dot{Q}_{Bd}^T = \tfrac{1}{2} \Omega_{TBd}^{Bd} Q_{Bd}^T \tag{15}$$

$$\Omega_{TBd}^{Bd} = \begin{bmatrix} 0 & -\omega_x^{Bd} & -\omega_y^{Bd} & -\omega_z^{Bd} \\ \omega_x^{Bd} & 0 & -\omega_z^{Bd} & \omega_y^{Bd} \\ \omega_y^{Bd} & \omega_z^{Bd} & 0 & -\omega_x^{Bd} \\ \omega_z^{Bd} & -\omega_y^{Bd} & \omega_x^{Bd} & 0 \end{bmatrix}; \qquad \omega_{TBd}^{Bd} = \begin{bmatrix} \omega_x^{Bd} \\ \omega_y^{Bd} \\ \omega_z^{Bd} \end{bmatrix} \tag{16}$$

$$\dot{\omega}_{TBd}^{Bd} = I_{Bd}^{-1} (M_d^{Bd} - [\omega_{TBd}^{Bd} \times] I_{Bd} \omega_{TBd}^{Bd}) \tag{17}$$

Therefore, given the initial conditions for the attitude of the hose and the drogue relative to the tangent frame, it is possible to compute the time history using the kinematic equations of motion (12), (14), (15), and (17) through substitution of Eq. (1) into Eqs. (10) and (11) to define the aerodynamic forces and moments and the resulting total forces and moments acting on the hose and on the drogue.

Equation (1) requires as inputs the actuator positions u as well as the local angle of attack α and sideslip β, which are calculated using the velocity of the drogue relative to the air-mass motion. Given a vector V_W^T representing the wind vector in the local tangent frame, the angle of attack and sideslip are calculated using the difference between the wind velocity and the inertial velocity, as defined in Eqs. (18) and (19), with wind relative drogue velocity V_{Wd} defined in Eq. (20). The drogue velocity relative to the local tangent frame V_d^{Bd} is calculated using the instantaneous orientation, and the velocity of the hose and drogue is provided without proof, as shown in Eq. (21). In the simulation, a DFRC wind-gust model is used to generate disturbances. The instantaneous wind gust is simply added to the wind vector V_W^T to calculate the instantaneous angle of attack and sideslip acting on the drogue:

$$\alpha = \tan^{-1}\left(\frac{V_{Wdz}}{V_{Wdx}}\right) \tag{18}$$

$$\beta = \sin^{-1}\left(\frac{V_{Wdy}}{\|V_{Wd}\|}\right) \tag{19}$$

$$V_{Wd} = \begin{bmatrix} V_{Wdx} \\ V_{Wdy} \\ V_{Wdz} \end{bmatrix} = C_T^{Bd} V_W^T - V_d^{Bd} \tag{20}$$

$$V_d^T = C_{Bl}^T [\omega_{TBl}^{Bl} \times] l^{Bl} + C_{Bd}^T [\omega_{TBd}^{Bd} \times] L_{\text{c.g.}}^{Bd} \tag{21}$$

The dynamics defined are integrated through a Runge–Kutta scheme. To test actuator dynamics limits, a set of simple first-order lag actuator states was added to the dynamics. For each actuator i of the four drogue actuators, Eq. (22) was used, where τ represents the actuator time constant, u_i is the true actuator position in degrees, and u_{cmd} is the commanded actuator position from the regulator. The actuators were also rate-limited by ensuring that $|\dot{u}_i| \leq \dot{u}_{\max}$ for the given actuator:

$$\dot{u}_i = \frac{-1}{\tau} (u_i - u_{\text{cmd}}) \tag{22}$$

Using the simulation with the linearized aerodynamics and actuator positions, a steady-state catenary position is calculated based on fixed actuator positions and steady-state air velocity. The initial position of the drogue is set to the assumed steady-state position without a neutral command input, corresponding to hole 9 in the data set. Each actuator was tested in the range from hole 1 to hole 9 in increments of two holes. Each actuator was tested individually. Then combinations of actuators were tested. All actuators were tested symmetrically. Then opposing actuators were tested asymmetrically. Finally, neighboring actuators were tested symmetrically. With each actuator command set, the simulation was started and the drogue was allowed to stabilize, given the fixed actuator positions. The results are

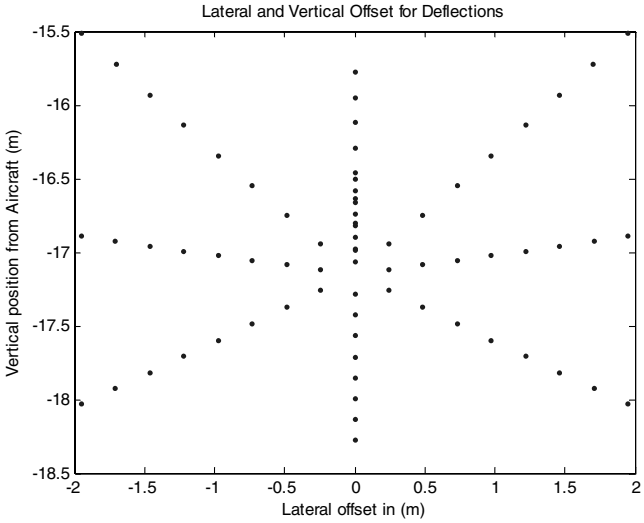

Fig. 8 Steady-state catenary results for linearized dynamics using two struts.

presented in Fig. 8, which shows the maximum steady-state position that can be maintained with any combination of actuator positions.

The test was repeated multiplying the actuator coefficient values of Table 3 by a factor of 1.38 to simulate a controllable drogue with three struts used at each actuator location. This test is performed to show how much more performance may be easily gained by adding more strut arms to each actuator. The results show that the maximum lateral position of ± 3 m and a maximum vertical position of ± 2 m can be achieved by using three strut arms.

As a final validation test, the linearized aerodynamics are replaced in the simulation with a table lookup of the actual data recorded in the wind tunnel. Linear interpolation was used to derive values between test points for the simulation. The results for the maximum catenary position are shown in Fig. 9. This data set has nearly the same maximum catenary position as the linearized model shown in Fig. 8. However, the nonlinearities appear to cause a certain twist in the catenary position angles. This is likely caused by the weak rolling moment that was only partially captured by the linearized dynamic model.

C. Regulator Design

A control law was designed using an LQR. In this case, the goal was to devise a regulator that would maintain a relative fixed position behind the tanker and dampen out disturbances due to wind gusts or the receiver forebody effect. The control law was given knowledge of the drogue mass properties, but no knowledge of the hose was assumed, since these properties cannot be known precisely, given current hose-reel technology and manufacturing variations.

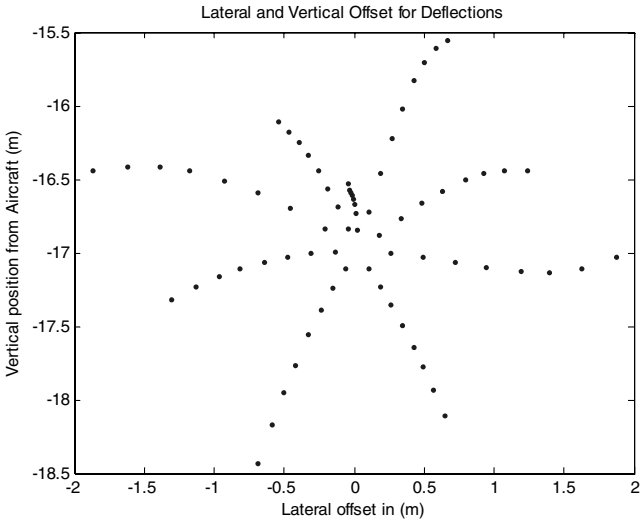

Fig. 9 Steady-state catenary position for two strut arms using nonlinear aerodynamic-data tables.

The regulator described can be reduced to a system to dampen angular rates and accelerations while holding a specified angle of attack and angle of sideslip. A set point was defined based on the natural steady-state catenary position behind the tanker. To estimate the drogue position, a position measuring device [such as a differential Global Positioning System (DGPS) receiver or an electro-optical camera system on the drogue looking at either the tanker or the receiver] is required. The DGPS solution requires a data link on the drogue communicating with a DGPS-enabled Global Positioning System (GPS) receiver on the tanker or receiver aircraft. An inertial measurement unit (IMU) is assumed to be on the drogue to measure high rate acceleration and angular rate that could be integrated to provide a full navigation state. A method for measuring air data using static and dynamic pressure ports on the surface of the shroud can be used to provide true airspeed.

Using the linearized dynamics, an LQR is designed to track relative position. The LQR chooses the control that minimizes the cost criterion,

$$J = \int_{t=0}^{\infty} (x^T Q^{-1} x + u^T R^{-1} u)\, \mathrm{d}t \tag{23}$$

subject to the linear dynamic constraints:

$$\dot{x} = Ax + Bu_{\text{act}} \tag{24}$$

In this case, the state variables are

$$x = \begin{bmatrix} P_E \\ P_D \\ V_E \\ V_D \\ \alpha \\ \beta \\ \omega^B_{IBy} \\ \omega^B_{IBz} \end{bmatrix} - \begin{bmatrix} \bar{P}_E \\ \bar{P}_D \\ 0 \\ 0 \\ \alpha_0 \\ 0 \\ 0 \\ 0 \end{bmatrix} \tag{25}$$

The state consists of the error between the east position P_E and the desired east position $\bar{P}_E$, and the error between the down position P_D and the desired down position $\bar{P}_D$. The state also consists of the east and down velocities (V_E and V_D), the angle of attack and sideslip, and the inertial pitch rate and yaw rate. The regulator works to drive the system to the desired position while driving the velocity, sideslip, and inertial angular velocities to zero. The angle of attack is driven to a trimmed value. Note that the vertical position and longitudinal position are coupled in this model and in the real drogue system. Since the hose is a fixed length, any increase in vertical position must be accompanied by an increase in the longitudinal position. Therefore, only vertical and horizontal control is necessary for station keeping, since commanding a vertical or horizontal position automatically constrains the longitudinal position.

The equations of motion are formulated in the north–east–down (NED) frame for convenience. In reality, the equations of motion will be formulated using relative position behind the tanker in the tanker body frame. Currently, the tanker is aligned with the NED frame for the purposes of this simulation.

The dynamics are depicted in Eq. (26).

$$A = \begin{bmatrix} 0_{2\times2} & I_{2\times2} & 0_{2\times2} & 0_{2\times2} \\ 0_{2\times2} & 0_{2\times2} & A_{F\text{aero}} & 0_{2\times2} \\ 0_{2\times2} & 0_{2\times2} & 0_{2\times2} & I_{2\times2} \\ 0_{2\times2} & 0_{2\times2} & A_{\omega\text{aero}} & -b_f I_{2\times2} \end{bmatrix} \tag{26}$$

The aerodynamic terms are defined as in Eq. (27), where which the term $\bar{q}$ is the dynamic pressure, m_d is the mass of the drogue, C_B^{NED} rotates the drogue body frame to the NED frame, and

$$A_{F\text{aero}} = \frac{\bar{q}}{m_d}\begin{bmatrix} 0 & 0 & 1 \\ 0 & 1 & 0 \end{bmatrix} C_B^{\text{NED}} \begin{bmatrix} C_{D\alpha} & C_{D\beta} \\ C_{Y\alpha} & C_{Y\beta} \\ C_{L\alpha} & C_{L\beta} \end{bmatrix} \tag{27}$$

The rotational aerodynamics are defined in Eq. (28), where which the rotational inertia of the drogue is defined as I_{BB}^B. The definition of angle of attack and sideslip as the integral of inertial angular velocity as defined in these dynamics is an approximation. The friction in the ball joint b_f is also an approximation to the resistance that the ball joint will exert to moments acting on the drogue:

$$A_{\omega\text{aero}} = \bar{q}\begin{bmatrix} 0 & 0 & 1 \\ 0 & 1 & 0 \end{bmatrix} (I_{BB}^B)^{-1} \begin{bmatrix} C_{rm\alpha} & C_{rm\beta} \\ C_{pm\alpha} & C_{pm\beta} \\ C_{ym\alpha} & C_{ym\beta} \end{bmatrix} \tag{28}$$

The control sensitivity matrix B is defined in Eq. (29):

$$B = \begin{bmatrix} 0_{2\times4} \\ B_F \\ 0_{2\times4} \\ B_\omega \end{bmatrix} \tag{29}$$

The linear actuation terms are defined in Eq. (30), and the rotational control surfaces are defined in Eq. (31). It is important to note that the rotation matrix takes into account the orientation of the drogue control actuators relative to the NED frame. However, the linearized data do not take into account the effect of gravity on drogue effectiveness:

$$B_F = \frac{\bar{q}}{m_d}\begin{bmatrix} 0 & -1 & 0 \\ -1 & 0 & -1 \end{bmatrix} C_B^{\text{NED}} \begin{bmatrix} C_{Du} \\ C_{Yu} \\ C_{Lu} \end{bmatrix}_{3\times4} \tag{30}$$

$$B_\omega = \bar{q}\begin{bmatrix} 0 & -1 & 0 \\ 0 & 0 & -1 \end{bmatrix} (I_{BB}^B)^{-1} \begin{bmatrix} C_{rmu} \\ C_{pmu} \\ C_{ymu} \end{bmatrix}_{3\times4} \tag{31}$$

The LQR design assumes perfect knowledge of the aerodynamics and actuator position. For simplicity, the system does not account for actuator lag. Later results introduce the simple first-order lag described previously. For the LQR design, the following weightings were used:

$$Q = \begin{bmatrix} 1.0e^{10} I_{2\times2} & 0_{2\times2} & 0_{2\times2} & 0_{2\times2} \\ 0_{2\times2} & 1.0e^{-2} I_{2\times2} & 0_{2\times2} & 0_{2\times2} \\ 0_{2\times2} & 0_{2\times2} & 1.0e^{-2} I_{2\times2} & 0_{2\times2} \\ 0_{2\times2} & 0_{2\times2} & 0_{2\times2} & 1.0e^{-4} I_{2\times2} \end{bmatrix} \tag{32}$$

$$R = \frac{1}{2.5e^{-7}} I_{4\times4} \tag{33}$$

The simulation effectively weights differences in position that are greater than any of the other states.

IV. Simulation Results

Figure 10 shows the block diagram of the integration of the control law with the simulation model. A set point of a desired catenary position is specified for the drogue. The set point is differenced with the current drogue location and the difference is given to the regulator. The simulation currently assumes perfect measurements. The regulator sets actuator positions that are used to drive the numerical simulation of the drogue. The simulation has the ability to incorporate the aerodynamic-data tables, the polynomial curve fits, or the linearized aerodynamics as the reference model. Results presented in this report used the linearized aerodynamics. The simulation was integrated at a 0.025 time step over 15 to 20 s runs. The control law operated at 10 Hz.

Disturbances were introduced to the drogue model using the F-18 receiver forebody effects and the DFRC wind-turbulence model. The wind-turbulence model uses a random number generator passed through a shaping filter to generate random turbulence proportional to the wind turbulence expected for a given altitude and airspeed. Turbulence is classified by strength as light, moderate, or heavy. The output of the turbulence model is a three-axis wind-vector velocity representing the size of the wind relative to the true airspeed. The wind-gust velocities were added to the airspeed at the drogue, effectively modifying the local angle of attack and sideslip on the drogue. For the results presented here, moderate turbulence at 125 KIAS is used. Gusts in excess of 5 m/s or 8% of the total airspeed (66.87 m/s) occur frequently at this setting.

Receiver forebody effects were introduced that match those published previously by Vassberg et al. [2]. The Vassberg et al. data table provides estimates of the localized u, v, and w (the three components of airspeed) in an area around the nose of an F-18 aircraft with a deployed refueling probe. For the simulation in this paper, the table values are normalized to the freestream airspeed velocity and the normalized values are assumed to be constant with respect to airspeed. The freestream velocity applied was 125 KIAS to generate changes in the airspeed in the vicinity of the F-18 forebody. Figure 11 shows the effective wind gust generated by an approaching F-18 on the drogue. The F-18 probe tip approaches the desired catenary position from a starting location below and to port of the drogue at a rate of 3 ft/s, which is a typical approach velocity. The right-hand plot shows the effect of the approaching F-18 on the air velocity around the drogue. The forebody effects induce a wind that pushes the drogue up and to starboard (east) of the F-18.

A worst-case simulation capability is presented. The drogue is started with a 1 m offset from the desired vertical condition. Moderate turbulence and the F-18 receiver forebody effects are used to perturb the dynamics. The motions of the drogue without the controller and with the controller are presented in Fig. 12. The left plots show that the combined effect of moderate wind and receiver forebody may generate drogue motion of 4 m from the desired catenary when no control is applied. However, when the control law is applied, it is able to attenuate the effects. The control law was shown to drive the error to within ±5 cm of the desired position within 5 s from the start of the simulation, despite the initial offset, moderate wind gusts, and the receiver forebody effects.

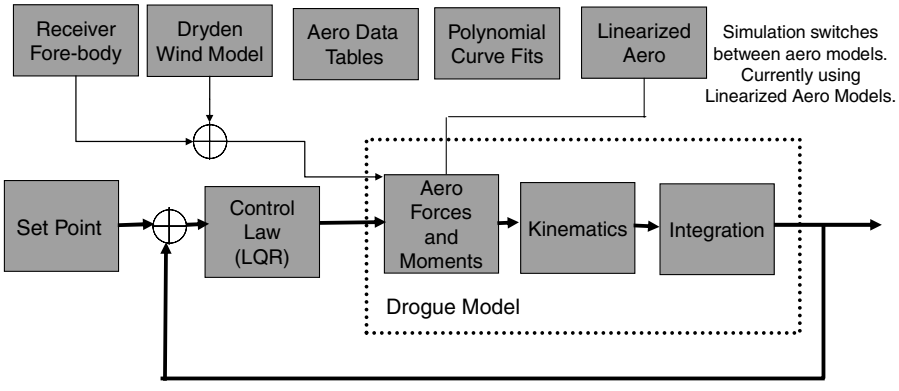

Fig. 10 Control simulation model.

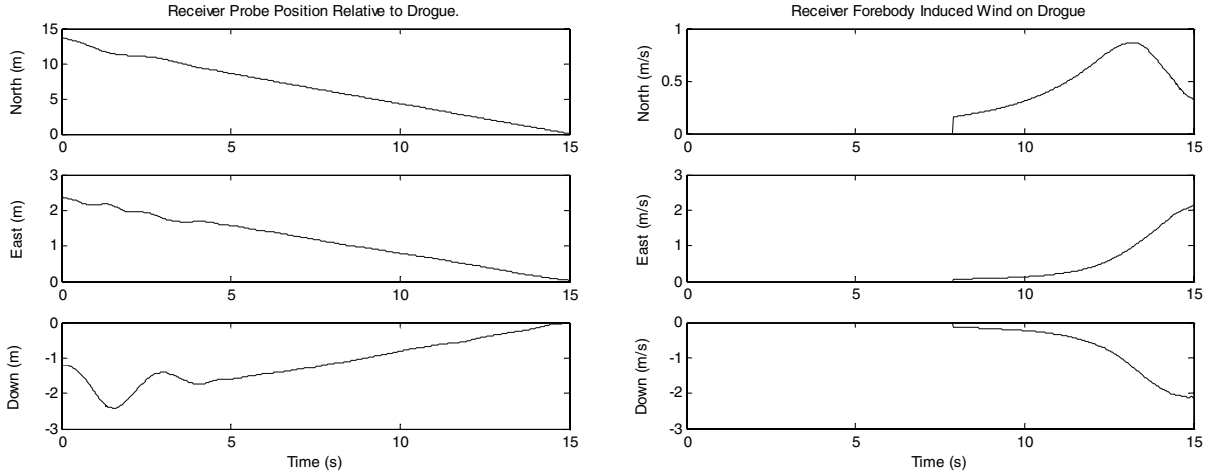

Fig. 11 F-18 probe tip position relative to desired catenary (left) and induced wind disturbance on drogue (right).

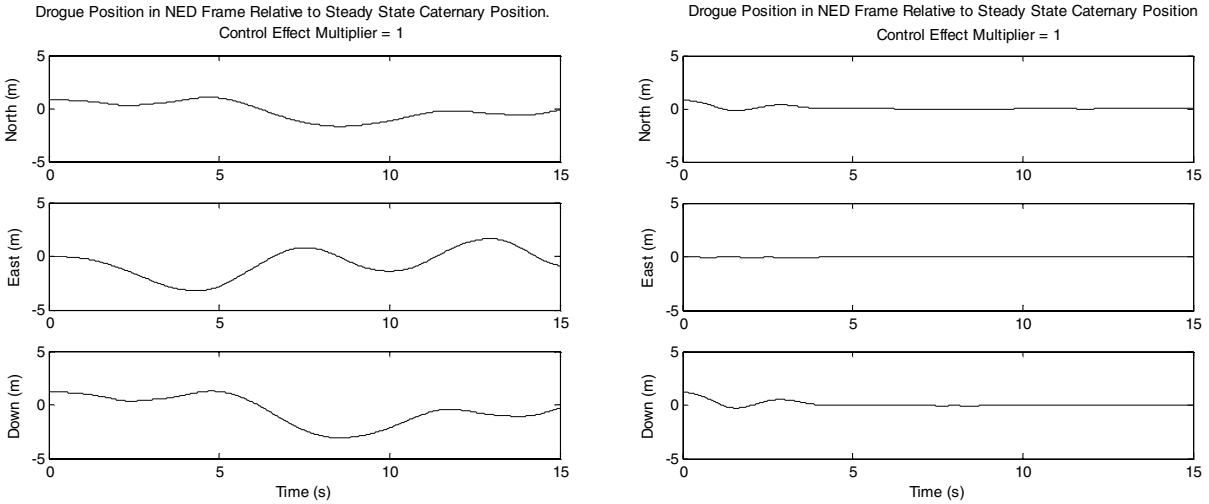

Fig. 12 Drogue position error without control (left) and with control (right).

Actuator bandwidth limits are introduced to demonstrate performance using real-world actuators using minimum bandwidth to minimize power requirements. Since force times velocity equals power, and since the amount of force required for maneuvering the drogue is fixed for this canopy and actuator design, then minimum power requirements are achieved when the actuator rate is minimized. In a previous section, several linear rate limits were established. The rates corresponded to angular rates between the leading and trailing edges of 10, 25, and 50 deg/s, respectively. The goal was to demonstrate control authority with disturbances using the different rates.

Each actuator was modeled as a first-order lag. The time constant on the actuator corresponded to the frequency at which a given command would be attenuated by 3 dB. For the low-speed drogue, the 3 dB attenuation of actuator command occurred at 0.7, 1.5, and 3 Hz for the 10, 25, and 50 deg rate limit. The lag was modeled in both the nonlinear dynamics and in the control law. It was assumed that the control law has knowledge of the actuator lag. Future work will test the robustness of this assumption.

Control was demonstrated for the lowest actuator rate of 10 deg/s, corresponding to an actuator bandwidth of 0.7 Hz. Results showed that zero mean error could be achieved within the 5 cm tolerance for the case of light turbulence, with the addition of receiver forebody effects, and combined light turbulence with the receiver forebody effects, although a longer settling time was required.

V. Conclusions

A controllable drogue concept was presented and shown to be feasible for flight. The aerodynamic coefficients of canopy manipulation were measured in the wind tunnel. These results showed that nearly linear vertical and side forces were generated with respect to leading- and trailing-edge strut-angle separation. A numerical simulation was built based on these results, which showed that ± 2 m of horizontal and ± 1.5 m of vertical deflection could be sustained by a low-speed drogue relative to the natural catenary position. A control law was implemented based on the proposed canopy-manipulation scheme. The control law was shown to attenuate effects due to offsets from a desired catenary position, moderate wind gusts from the DFRC model, and receiver forebody effects from an approaching F-18 aircraft.

Simulation results show that low-bandwidth actuators could be used to achieve these results. Actuators would be required to supply the 120 lb of force required at each of the four locations through either direct drive or by designing an actuation method to supply the necessary mechanical advantage. Rate limits of 15 deg/s of angular separation between struts were sufficient to compensate for the worst-case scenario presented. It is conceivable that batteries could be stored within the volume of the shroud to power the drogue system. Some drogues are equipped with a Pelton wheel generator, which could also provide significant power at the applicable airspeeds. A combination of both a generator and batteries could provide power for the drogue indefinitely. This would eliminate the need to modify hose designs to include a power line, enabling users to bolt on this drogue to any existing refueling system.

The drogue would also be equipped with a navigation system. A simple IMU is the minimal requirement to provide measurements of rate to stabilize the drogue. Adding a differential GPS system such as those currently under consideration for boom-receptacle-style refueling would allow the drogue to estimate position relative

to the tanker or the approaching receiver. Alternatively, or in addition, an electro-optical system on the drogue could be used to track an approaching receiver or the tanker. In both cases, estimating relative position would be straightforward using existing systems and would not require significantly more power or volume within the drogue.

The benefits of this viable solution to a controllable (dampened and/or autonomous tracking) drogue directly relates to mission accomplishment and conservation of military resources by reducing aerial refueling cycle time and minimizing or eliminating probe–drogue-related mishaps. This improvement is accomplished by the dampening of receiver-induced drogue oscillations enabled by the application of the aforementioned technologies. The logistics associated with refueling drogue material will be minimally affected in that the components that are to be used to achieve this controllability are modularized and packaged (including a power-generating system) to physically fit within the drogue. This modular package would not be limited to one particular drogue model, but would be a bolt-on capability for any drogue in present use aboard any tanker aircraft and would require no other hardware changes for either the tanker or receiver.

A final significant advantage of this drogue concept is safety. In particular, with both the ability to detect and maneuver around an approaching receiver, a controllable drogue has the potential to mitigate potentially hazardous scenarios such as a receiver approaching too quickly. Finally, if the drogue is damaged, it simply reverts to the normal drogue with performance that is already well understood.

Acknowledgments

The authors wish to thank the U.S. Navy for the support of this project under contract N68335-08-C-0083. The authors wish to acknowledge John Vassberg for the use of the F-18 aerodynamic model. The authors also wish to thank Jim Murray of NASA Dryden Flight Research Center for his insight into the NASA flight tests.

References

[1] Dryden, H. L., "A Review of the Statistical Theory of Turbulence," *Turbulence–Classic Papers on Statistical Theory*, Interscience Publishers, New York, 1961.

[2] Vassberg, J., Yeh, D., Blair, A., and Evert, J., "Numerical Simulations of KC-10 In-Flight Refueling Hose-Drogue Dynamics with an Approaching F/A-18D Receiver Aircraft," 23rd AIAA Applied Aerodynamics Conference, AIAA Paper 2005-4605, June 2005.

[3] Knacke, T. W., *Parachute Recovery Systems Design Manual*, Para Publishing, Santa Barbara, CA, 1992.

[4] Eichler, J., "Dynamic Analysis of an In-Flight Refueling System," *Journal of Aircraft*, Vol. 15, No. 5, May 1978, pp. 311–318. doi:10.2514/3.58361

[5] Zhu, Z. H., and Meguid, S. A., "Elastodynamic Analysis of Aerial Refueling Hose Using Curved Beam Element," *AIAA Journal*, Vol. 44, No. 6, June 2006, pp. 1317–1324. doi:10.2514/1.17311

[6] Ribbens, W. B., Saggio, F., Wierenga, R., and Feldmann, M., "Dynamic Modeling of an Aerial Refueling Hose and Drogue System," 25th AIAA Applied Aerodynamics Conference, Miami, FL, AIAA Paper 2007-3802, June 2007.

[7] Ro, K., and Basaran, E., "Aerodynamic Investigations of Paradrogue Assembly in Aerial Refueling System," 44th AIAA Aerospace Sciences Meeting and Exhibit, AIAA Paper 2006-855, Jan. 2006.

[8] Ellsworth, J. A., Fox, W. R., Lovendahl, D. E., and Moore, J. E., "Guided Drogue Flight Test Report," U.S. Department of the Navy TR E-23027, Jan. 1978.

[9] Hansen, J. L., Murray, J. E., and Campos, N. V., "The NASA Dryden Flight Test Approach to an Aerial Refueling System," NASA Dryden Flight Research Center TM-2005-212859, Edwards, CA, Feb. 2005.

[10] *CRC Handbook of Mechanical Engineering*, CRC Press, Boca Raton, FL, 2003.

[11] Zipfel, P. H., *Modeling and Simulation of Aerospace Vehicle Dynamics*, AIAA Education Series, AIAA, Reston, VA, 2000.